https://doi.org/10.3311/PPme.42144



**Periodica Polytechnica Mechanical Engineering**, 69(4), pp. 377–391, 2025

# Compressive Properties of Al99.5 Matrix Syntactic Foams Reinforced by SiC Particles in the Matrix

János Endre Maróti[1, 2*], Imre Norbert Orbulov[1, 2]

[1] Department of Materials Science and Engineering, Faculty of Mechanical Engineering, Budapest University of Technology and Economics, Műegyetem rakpart 3., H-1111 Budapest, Hungary
[2] MTA-BME Lendület "Momentum" High-performance Composite Metal Foams Research Group, Műegyetem rakpart 3., H-1111 Budapest, Hungary
[*] Corresponding author, e-mail: maroti.janos.endre@gpk.bme.hu

Received: 07 September 2025, Accepted: 25 September 2025, Published online: 26 November 2025

**Abstract**

Reinforced metal matrix syntactic foams (rMMSFs) were produced by liquid-state, low-pressure vacuum infiltration. Technical purity Al99.5 aluminum alloy was used as the matrix material, and ceramic hollow spheres (CHSs) with Ø2.24±0.13 mm diameter were applied as a filler material. The matrix was reinforced by 0.6 nominal size SiC with seven different volume fractions of the reinforcing material relative to the matrix material's volume: 0 vol%, 5 vol%, 10 vol%, 15 vol%, 20 vol%, 25 vol%, and 30 vol%, respectively. The samples were investigated structurally and mechanically. Based on the microscopic investigation, the liquid-state, low-pressure vacuum infiltration was found to be a good production method of the rMMSFs; no traces of reactions between the components had been found. Based on the results of the standardized compressive test, the specific compressive strength and specific structural stiffness of rMMSFs were significantly increased for each reinforcement volume fraction, and even a 63.2±8.1% improvement can be achieved in the specific compressive strength compared to the unreinforced (UR) samples. The specific plateau strength and the specific energy absorption were improved with a 15 vol% or above reinforcement volume fraction compared to the UR foams. The decrement was caused by the stress-concentrating particles, and this effect could only be equalized by higher reinforcement content. The failure modes of the MMSFs were dependent on the dual composite properties of rMMSFs. The failure of the reinforced samples was indicated by plastic collapse followed by the appearance of a cleavage band and its widening.

**Keywords**

reinforced, characterization, composites, metal matrix syntactic foam

## 1 Introduction

The first artificial foams were produced from polymers and were later followed by the development of conventional metal foams to achieve improved mechanical properties. Metal foams are commonly categorized into three main groups: (i) open cell metal foams, (ii) closed cell metal foams, and (iii) closed cell metal foams in which the porosity is generated by the incorporation of a secondary phase. The latter are referred to as metal matrix syntactic foams (MMSFs).

In MMSFs, low-density metals with excellent specific properties are used as the matrix material. Aluminum [1–5] is most frequently employed due to its low density, good castability, and excellent mechanical properties, which can be further improved in certain alloys by heat treatment. Magnesium [6–11] can also be used because of its low density and low melting temperature; however, its high chemical reactivity and relatively high cost can limit its widespread application. In addition, steel [12–18] (high strength, cheap but high density), titanium [19–21] (acceptable density, good specific properties, expensive), and zinc [22–25] (high density) matrices have also been reported in the literature.

The porosity and superb specific mechanical properties of MMSFs can be granted by hollow spheres and porous particles. The hollow particles are engineered ceramic [1] or metallic hollow spheres made of $Al_2O_3$ [26–31], glass [7, 31–34] or steel [14, 17, 35–37], whereas porous particles can be expanded perlite [38-43], expanded glass [44–47] or expanded clay aggregates [48–52].

A variety of manufacturing routes have been developed for syntactic metal foams. The most common include stir casting [53–55], pressure infiltration (with or without

**Cite this article as:** Maróti, J.E., Orbulov, I. N. "Compressive Properties of Al99.5 Matrix Syntactic Foams Reinforced by SiC Particles in the Matrix", Periodica Polytechnica Mechanical Engineering, 69(4), pp. 377–391, 2025. https://doi.org/10.3311/PPme.42144

vacuum assistance) [8, 56], powder metallurgy [57, 58], and gravity casting [15, 59].

MMSFs are characterized by a high specific energy absorption capacity and excellent specific mechanical properties, which make them attractive for automotive [60–63] and defense applications [64–66], such as collision energy dissipation, mass reduction leading to lower fuel consumption, and ballistic or blast protection. Due to their favorable thermal [22, 67–69] and acoustic insulation capabilities, they are also applied in the construction industry.

Although MMSFs offer numerous advantages over conventional metal foams and bulk metals, a significant limitation is the cost of certain filler materials, particularly engineered ones (e.g., CHS). The porous particles are less expensive than their engineered counterparts but exhibit inferior mechanical performance, which is reflected in the produced MMSFs.

Two main strategies have been reported to enhance the specific properties of MMSFs: (i) the use of higher strength fillers material, but it would further increase the production costs of the metal foams; and (ii) the application of stronger matrix materials, such as heat treated aluminum, steel (despite its high density), or titanium (despite its high cost), or composite matrices reinforced with ceramic particles (e.g., $Al_2O_3$ or SiC). Conventional closed cell metal foams with ceramic particle reinforced matrices have been described in the literature; however, to the best of the authors' knowledge, MMSFs reinforced by ceramic particles in their matrix have been reported only in the preliminary publication of the present authors [70] while the filler was a set of ceramic hollow spheres (CHSs. Compared with previous publications, a much wider investigation was presented on the effect of the amount of reinforcement on the specific mechanical properties.

## 2 Materials and methods

### 2.1 Materials

Technical purity Al99.5 purity aluminum alloy was used as the matrix material. Its nominal chemical composition is ≤0.25 wt.% Si, ≤0.4 wt.% Fe, ≤0.05 wt.% Cu, ≤0.05 wt.% Mn, ≤0.05 wt.% Mg, ≤0.07 wt.% Zn, ≥99.5 wt.% Al and its density is 2.7 $gcm^{-3}$. Aluminum and its alloys are excellent choices as matrix materials because they have low density, good casting and good specific mechanical properties.

Ceramic hollow spheres (CHS) were used as filler material. The CHSs' diameter was ∅2.24±0.13 mm, based on scanning electron microscopic measurements (on 500 randomly selected CHS), and their bulk density was 0.87±0.08 $gcm^{-3}$. Their material was high-purity grade $Al_2O_3$. The filler material is shown in Fig. 1.

The primary function of the filler phase is to effectively lower the foam's density, thereby imparting foam-like properties to the material. Specific properties improve as the density decreases (assuming constant strength), so the filler volume fraction was set relatively high at 64 vol%, guaranteed by a random, closely packed structure.

Technical grade SiC particles were used as reinforcing materials with a 0.597±0.11 mm size range (0.6 mm nominal size), shown in Fig. 2 The role of reinforcement is to further improve the specific mechanical properties and energy absorption of the reinforced metal matrix syntactic foams (rMMSFs). The reinforcement was chosen based on availability and its proven feasibility in producing metal matrix composites. The reinforcements were supplied by Granit Abrasive Ltd.

**Fig. 1** Macroscopic image of the applied filler material


**Fig. 2** Macroscopic image of the applied reinforcement particles: 0.6 mm nominal size of SiC

The main factor that was altered in our investigations as a research parameter was the volume fraction of the reinforcing material relative to the matrix material's volume (relative to the whole volume): seven different volume fractions were investigated: 0 vol%, 5 vol% (1.46 vol%), 10 vol% (2.92 vol%), 15 vol% (4.38 vol%), 20 vol% (5.84 vol%), 25 vol% (7.3 vol%) and 30 vol% (8.76 vol%), respectively.

The main goals of our investigation were (i) to judge the feasibility of the production with a high amount of reinforcing particles and (ii) to report the first results on the strength and energy absorption increment caused by various volume fractions of SiC particles. A summary of the used filler and reinforcing material, the applied volume fractions of the reinforcing particles, and the samples' relative densities (sample densities divided by the matrix material's density) are listed in Table 1. In the designations, the first part describes the reinforcing particle nominal size, and the second part describes the volume fraction of the reinforcing material relative to the matrix material's volume (For example, 0.6–15 designates an rMMSF reinforced by 0.6 nominal size SiC particles with 15 % volume fraction).

### 2.2 Production

The specimens were produced by liquid-state, low-pressure vacuum infiltration. The filler and reinforcement particles were mechanically stirred directly in a steel mold until a homogenous distribution was achieved. The production was considered successful if the specimens' densities differed from each other by no more than 10%. To facilitate the easy removal of the samples, the inner walls of the mold were treated with graphite (N-77 graphite spray, DUECI ELECTRONIC s.n.c.). A stainless-steel mesh and an alumina ($Al_2O_3$) quilt were positioned on top of the mixture to inhibit the displacement of the filler and reinforcement phases, which could otherwise compromise the uniformity of the final product. Following this preparation, the solid matrix material block was loaded into the mold. The entire setup was placed in an infiltration furnace, where it was initially heated to 600 °C for 1.5 h till the vacuum was built up to $10^{-4}$ Pa. Subsequently, the temperature was elevated to 750 °C and held constant for 1 h, while the matrix block melted. Inert argon gas at a pressure of 500 kPa was then applied for 5 s to drive the molten matrix into the interstitial spaces among the filler and reinforcing components. To prevent unwanted chemical interactions among the constituents, the assembly was rapidly cooled by room-temperature water.

### 2.3 Testing methods

Microstructural analyses of the fabricated rMMSF specimens were carried out using an Olympus PMG3 optical microscope, an Olympus SZX16 stereomicroscope, and a Zeiss EVO MA10 SEM. Sample preparation followed a standardized three-step procedure: (i) initial grinding was performed using SiC abrasive papers with P120, P320, P600, P1200, P2400 and P4000 grade (90 s, 20 N load, 220 rpm, counter-clockwise rotation); (ii) this was followed by polishing with 6 μm and 3 μm diamond suspensions, each for 10 min under a 25 N load at 150 rpm, also counter-clockwise; (iii) a final polishing step employed a 0.05 μm $SiO_2$ suspension for 5 min under a 25 N load at 125 rpm, with clockwise rotation.

The compressive properties were measured by an MTS810 universal hydraulic testing machine between two flat steel plates. The machine was equipped with a 250 kN load cell, and the testing was conducted at a constant crosshead speed of 3 mm/min, with samples compressed to a minimum of 50% engineering strain for comparability, following the ISO 13314:2011 standard [71]. Kolofol Teflon foil was placed between the sample surfaces and the plates to reduce friction during testing. The specimens were cubic with 25 mm edge lengths. Three samples were tested for each material configuration.

**Table 1** Summary of the used filler and reinforcing material, the applied volume fraction of the reinforcement, and the samples' relative density

| Designation | CHS filler | Reinforcement | | | Relative density $\rho rel$ (1) |
|---|---|---|---|---|---|
| | Diameter $D$ (mm) | Size $d$ (mm) | Material | Vol% | |
| UR | 2.24±0.13 | Unreinforced | - | 0 | 0.622±0.009 |
| 0.6–5 | | 0.597±0.11 (0.6 nominal size) | SiC | 5 | 0.644±0.007 |
| 0.6–10 | | | | 10 | 0.666±0.016 |
| 0.6–15 | | | | 15 | 0.670±0.014 |
| 0.6–20 | | | | 20 | 0.714±0.032 |
| 0.6–25 | | | | 25 | 0.704±0.036 |
| 0.6–30 | | | | 30 | 0.706±0.033 |

From the force-displacement data, the engineering stress–engineering strain curves were calculated, from which the following key mechanical properties were extracted: compressive strength ($\sigma_C$ - defined as the stress at the first peak following the elastic region), plateau stress ($\sigma_{PLT}$ – the average stress between 20% and 40% strain), energy absorption ($W_{50}$ – the area under the stress–strain curve up to 50% strain), and structural stiffness (S, the slope of the initial linear portion of the curve). In this study, these mechanical properties were evaluated in their specific form, normalized by the rMMSFs' density ($\rho$).

## 3 Results and discussion

### 3.1 Microstructural features of the rMMSFs

First, the production technique's effectiveness and the specimens' microstructure were investigated. Based on the microstructural images (Fig. 3), the infiltration process yielded excellent results. The matrix material uniformly filled the spaces between the filler and the SiC reinforcement particles, with no signs of matrix penetration into the filler, nor any agglomeration of either the filler or the reinforcing phase. These observations confirm that liquid-state low-pressure vacuum infiltration is a highly efficient method for fabricating reinforced MMSFs.

The microstructure of rMMSFs was also investigated by SEM and EDS. The SEM images and EDS maps are shown in Fig. 4 and Fig. 5, respectively. These investigations confirm liquid state low-pressure infiltration as an adequate production method, with no unwanted voids being seen at the interface between the fillers and the matrix or between the reinforcement and the matrix.

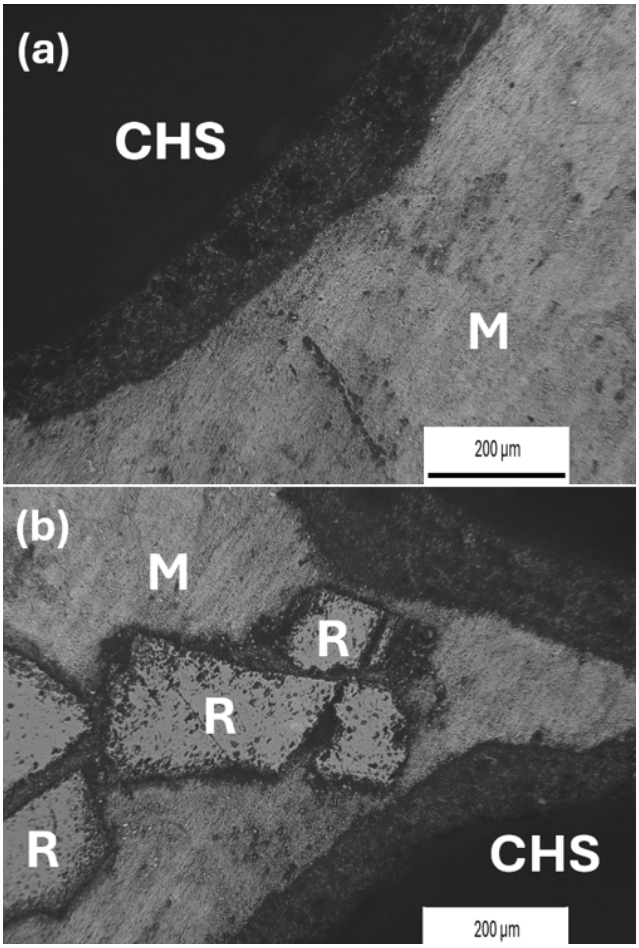


**Fig. 3** Microstructure of produced rMMSFs (a) unreinforced sample, (b) rMMSF reinforced by 15 vol% of 0.6 mm nominal size SiC (M – matrix, R – reinforcing particles, CHS – ceramic hollow spheres – please note that not all the particles have been labeled)

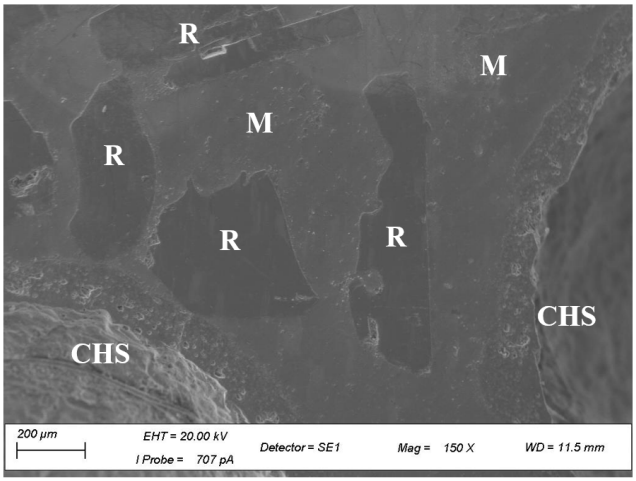


**Fig. 4** SEM image of the produced rMMSF in the case of rMMSF reinforced by 15 vol% of 0.6 mm nominal size SiC (M – matrix, R – reinforcing particles, CHS – ceramic hollow spheres – please note that not all the particles have been labeled)

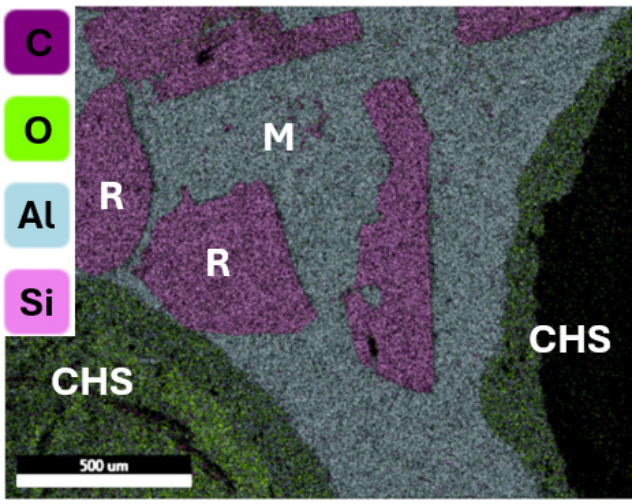


**Fig. 5** EDS map of the investigated rMMSF reinforced by 15 vol% of 0.6 mm nominal size SiC (M – matrix, R – reinforcing particles, CHS – ceramic hollow spheres – please note that not all the particles have been labeled)

Reactions between SiC, $Al_2O_3$, and Al99.5 mostly occur at elevated temperatures. SiC can react with molten aluminum above 900°C, forming aluminum carbide ($Al_4C_3$) and free silicon (Eq. (1)), which is undesirable due to $Al_4C_3$'s hygroscopic nature.

$$SiC + 4Al \rightarrow Al_4C_3 + Si \quad (1)$$

$Al_2O_3$ is highly stable and does not react chemically with aluminum under typical processing conditions, though interfacial diffusion or wetting may occur. There is no significant reaction between SiC and $Al_2O_3$ below 1600°C. At very high temperatures, however, minor interactions or complex phase formations might take place. Based on the production methods and the EDS measurements, no traces of reactions are expected nor have been found.

Please note that only the most representative images of the samples were inserted; however, all samples were examined, and their images and EDS maps of microstructure can be found in Appendix A and B.

### 3.2 Mechanical properties of rMMSFs

After the microstructural analysis, compressive tests were performed on the specimens. The evaluation focused on two main aspects: (i) the effect of reinforcement volume fraction, and (ii) the deviation from the unreinforced reference sample. The resulting engineering stress–strain diagram and the corresponding energy absorption values are presented in Fig. 6.

All plots follow the same layout: the average curves of the three compressive measurements for each composition are plotted by bold lines, while the corresponding standard deviations are shown by the shaded areas. The engineering stress-strain diagrams follow the classic behavior of CHS-filled MMSFs. The first peaks in the stress-strain diagrams were followed by sudden and significant drops of 6.3±1.3 MPa for the unreinforced cases and, on average 22.8±5.6 MPa for the reinforced cases.

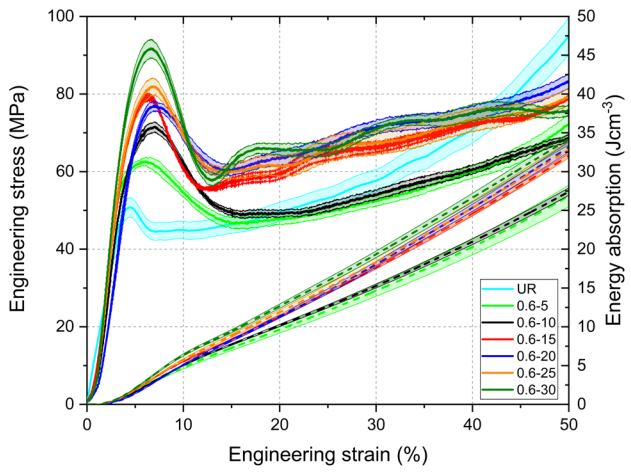


**Fig. 6** Engineering stress-engineering strain and energy absorption-engineering strain diagrams of the samples

The reason behind this is the initialization of the first compressive shear band in the samples. Investigating the diagrams further, it is clear that the plateau region of the curves increased continuously, since, except for the shear band section, it had retained its integrity and was capable of absorbing further energy. The corresponding energy absorption curves were almost straight, and no knee points were observed.

According to the ISO 13314:2011 standard [71] for the compressive testing of metallic foams, several characteristic properties can be derived from the diagrams to describe the samples' mechanical load-bearing and energy absorption capacity. The specific values (i.e., the property divided by the foam's density) of rMMSFs are the most significant. The numerical values are also presented in Appendices C and D.

#### 3.2.1 Compressive strength

First, the compressive strength – representing the load-bearing capacity of the rMMSFs – was examined in the case of Al99.5 matrix, CHS filler, and SiC reinforcement with a nominal particle size of 0.6 mm, when the reinforcement volume fraction is varied at 0 vol%, 5 vol%, 10 vol%, 15 vol%, 20 vol%, 25 vol%, and 30 vol%, respectively. The specific compressive strength values as a function of reinforcement volume fraction and the deviation from the reference (unreinforced MMSF) are shown in Fig. 7. The representation of the specific mechanical

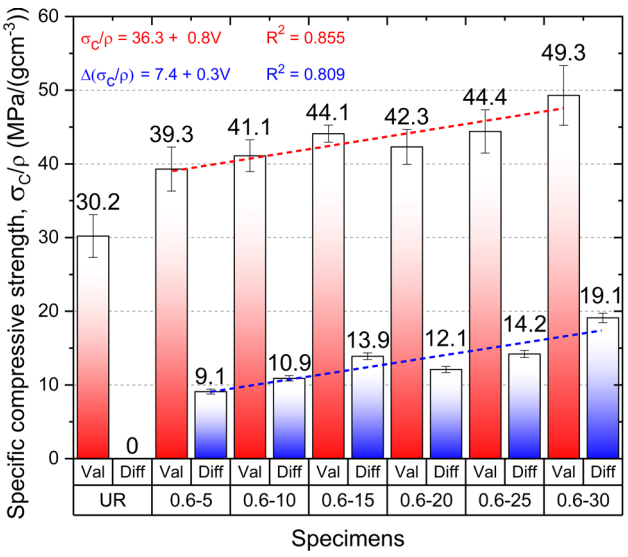


**Fig. 7** Specific compressive strength and its deviation from the unreinforced (UR) sample as a function of reinforcement particles' volume fraction

properties follows the same structure; the red bars represent the specific mechanical values as a function of reinforcement particles' volume fraction. The blue bars show the difference between the unreinforced and reinforced samples as a function of volume fraction of reinforcement.

The data clearly show that higher strengths were achieved in every case compared to the reference sample. A clear positive correlation was observed between the reinforcement volume fraction and the specific compressive strength. The values increase from 30.2±2.9 MPa·cm³/g (UR samples) to 49.3±4.0 MPa·cm³/g at 30% reinforcement content.

The only difference between the specimens was the amount of reinforcing material; therefore, the results indicate a strong relationship between reinforcement volume and mechanical performance. A linear relationship was fitted to the data. The goodness of the fitted curves (Eq. (2) and Eq. (3)) was found to be $R^2 = 0.855$ for the specific values and $R^2 = 0.809$ for the deviations.

$$\sigma_C / \rho = 36.3 + 0.8V \tag{2}$$

$$\Delta\left(\sigma_C / \rho\right) = 7.4 + 0.3V \tag{3}$$

It can be observed that the compressive strength increased in every examined case. This behavior is attributed to the double-composite nature of the investigated reinforced syntactic metal matrix foams. The role of the matrix material in metal foams is to absorb and transfer the load to the much stronger filler material. Selecting a matrix material with low density and excellent specific properties is advantageous. However, in this study, the matrix itself was already a composite structure, reinforced with SiC particles.

As a result, the difference in strength between the matrix and the filler materials was smaller. Consequently, the matrix material was capable of bearing significantly higher stresses, leading to a reduced load on the filler during loading. Thus, failure of the CHSs occurred at much higher stress levels compared to non-reinforced matrices, which is why there is a bigger strength drop after the first peak in the engineering stress-engineering strain diagrams.

### 3.2.2 Plateau strength

The next important mechanical property is the specific plateau strength. The plateau strength was defined as the average stress within the 20%–40% deformation range.

The plateau strength is strongly connected to the energy absorption of metal foams and is responsible for it during irreversible deformation and failure. The plateau region should be high, flat, and slightly increasing for high energy absorption. The specific plateau strength values and the deviation from the reference value are plotted in Fig. 8.

The UR – unreinforced – samples performed well. As can be seen in the engineering stress-engineering strain diagram (Fig. 6), the UR sample's plateau region was continuous, no break point was observed, and the sample showed a significant increase in the engineering stress in the high deformation range. Reinforced samples showed similar behaviour to the unreinforced sample, but the increment after the stress drop was not as high as in the case of the UR sample.

This phenomenon can again be attributed to the dual-composite nature of the specimens. As observed in the engineering stress–engineering strain curves, following the peak stress - which corresponds to the failure of the ceramic hollow spheres - a significantly greater stress drop occurs in the reinforced specimens compared to the unreinforced ones. Additionally, it was observed that the stress drop proceeds more gradually, and the slope of the plateau region is lower in the reinforced specimens.

The previously observed trend is again clearly visible, namely, that increasing the reinforcement volume fraction results in higher plateau strength. However, improvements were not observed in every case compared to the reference sample. In the case of 5 vol% and 10 vol%, there was a decrease (−4.1±0.5 MPa·cm³/g and −4.4±0.6 MPa·cm³/g, respectively), while the 15 vol%, 20 vol%, and 30 vol% samples show slight improvements (+2.1±0.1 MPa·cm³/g, +1.6±0.07 MPa·cm³/g, and +2.1±0.1 MPa·cm³/g).

The following linear correlations (Eq. (4) and Eq. (5)) were determined between the plateau strength (and its deviation

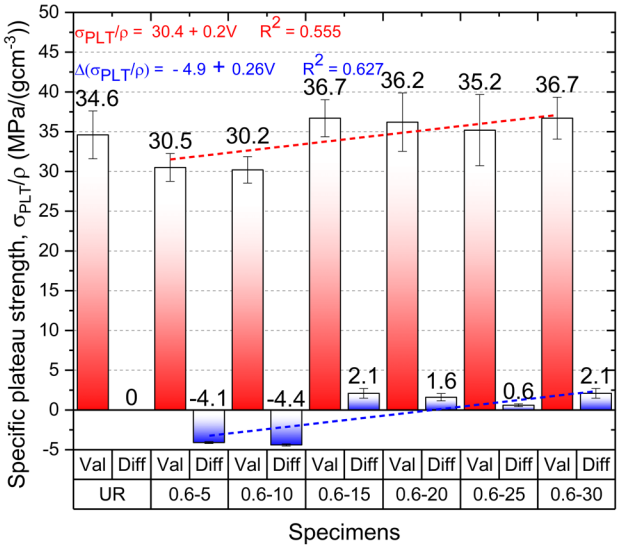


**Fig. 8** The specific plateau strength and its deviation from the unreinforced (UR) sample as a function of reinforcement particles' volume fraction

from the reference) and the volume fraction of SiC reinforcement with a nominal particle size of 0.6 mm within the examined range and parameters; the coefficients of determination were calculated to be $R^2$=0.555 and $R^2$=0.627, respectively.

$$\sigma_{PLT} / \rho = 30.4 + 0.2V \tag{4}$$

$$\Delta\left(\sigma_{PLT} / \rho\right) = -4.9 + 0.26V \tag{5}$$

After analyzing the results, it can be concluded that an increase in plateau strength was achieved using higher reinforcement volume fractions. Initial reinforcement addition (5 vol% – 10 vol%) may disrupt the structural integrity; technically, the reinforcement particles acted as stress concentrators during the plastic collapse of the samples, decreasing the plateau strength. Only higher reinforcement contents (≥ 15 vol%) begin to behave as reinforcing elements and increase the plateau strength. Based on this, the lowest limit of reinforcement volume fraction was 15 vol%.

The overall correlation is weaker ($R^2 \approx 0.56$–$0.63$), suggesting that plateau strength is less sensitive to the reinforcement volume or more influenced by local defects, deformation mechanisms, or microstructural features.

### 3.2.3 Energy absorption

Metal foams possess an exceptionally good specific energy absorption property. In industry, this property is most widely used (collision damping, bulletproof hulls, detonation-proof walls and ceilings, etc.), so the energy absorption is one of the most essential properties of metal foams. The energy absorption, by definition, is closely related to the shape of the plateau region in the engineering stress–engineering strain diagrams, because the energy absorption is the area under the engineering stress-engineering strain curve up to 50% engineering strain.

The specific energy absorption as a function of SiC volume fraction, along with the deviation from reference values, is shown in Fig. 9.

Compared to the reference specimen, reinforcement volume fraction limit was to 15 vol%, because improvements were achieved in the 15 vol%, 20 vol%, 25 vol%, and 30 vol% cases; the most significant improvement was achieved in the 30 vol% case with 127.1 J/g (7.6 %).

It can be observed that the energy absorption increases proportionally with the amount of reinforcement. Compared to the reference specimen, improvements were achieved in the 15 vol%, 20 vol%, 25 vol%, and 30 vol% cases; the most significant improvement was achieved in the 30 vol% case with 127.1 J/g (7.6 %).

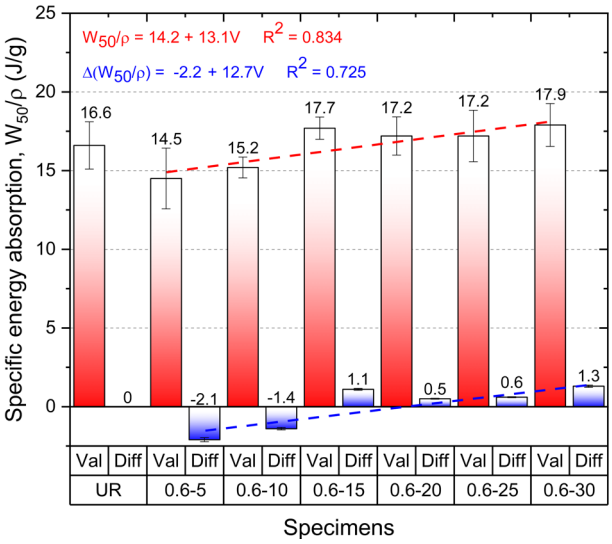


**Fig. 9** The specific energy absorption and its deviation from the unreinforced (UR) sample as a function of reinforcement particles' volume fraction

A linear fit was applied to the specific energy absorption results and to the difference from the reference, as the only varying parameter between the specimens was the amount of SiC reinforcement. The equations of the fitted curves, in the valid investigated region, are shown in Eq. (6) and Eq. (7) resulting in $R^2$=0.834 and $R^2$=0.725, respectively.

$$W_{50} / \rho = 14.2 + 13.1V \tag{6}$$

$$\Delta\left(W_{50} / \rho\right) = -2.2 + 12.7V \tag{7}$$

According to the definition of absorbed energy, as the integral of the engineering stress–strain curve over a deformation range of 0% to 50%, the results are significantly influenced by the compressive strength and plateau strength, and therefore by the shape of the deformation curve. Consequently, the findings of the previous sections also apply here: the matrix material in the reinforced syntactic foams demonstrates substantially higher strength than the matrix in unreinforced syntactic foams. As a result, it is capable of withstanding higher stress and distributes it more evenly and proportionally across the filler components, so the failure of the filler materials occurs later. However, in the later stage of deformation, higher mechanical properties can only be achieved by using a higher volume fraction of the reinforcing material.

### 3.2.4 Structural stiffness

The final mechanical property was the structural stiffness, defined as the slope of the elastic deformation region of the engineering stress–engineering strain curve.

The specific structural stiffness values (calculated by linear fitting on the initial, linear part of the compressive curves) and the deviation from the reference, unreinforced samples are shown in Fig. 10.

Improvement was achieved in every reinforced case. It can be concluded that the specific structural stiffness increases with the volume fraction of the reinforcing material. The highest difference (2.9 MPa·cm³/g, 34.5 %) was achieved in the case of 30 vol% reinforcement. This effect can be described by a linear relationship (Eqs. (8), (9)) with $R^2$=0.714 for the specific values and $R^2$=0.689 for the difference from the reference value.

$$S/\rho = 8.6 + 0.08V \tag{8}$$

$$\Delta(S/\rho) = 0.46 + 0.06V \tag{9}$$

These results can be attributed to the fact that the reinforced matrix material is capable of withstanding significantly higher stresses compared to the unreinforced matrix, as it can distribute the load between the filler materials, delaying failure. Consequently, the reinforced specimens exhibit elastic deformation even under greater loads, in contrast to their unreinforced counterparts.

### 3.3 Failure modes of rMMSFs

The failure modes of metal matrix syntactic foams under compressive loading can generally be categorized into two types: (i) cleavage along shear band(s) and (ii) plastic deformation. Cleavage failure typically involves the formation of a distinct shear band oriented at approximately 45° to the loading direction, where the maximum shear stress occurs. This mode is characteristic of MMSFs containing rigid fillers (such as ceramic hollow spheres), rigid matrix materials, and specimens with an aspect ratio greater than 1.5. In contrast, plastic deformation is more prevalent in MMSFs with less-rigid, lower-strength fillers (for example, light expanded clay agglomerate particles (LECAPs)), ductile matrices with low proof strength, and aspect ratios of 1.5 or less.

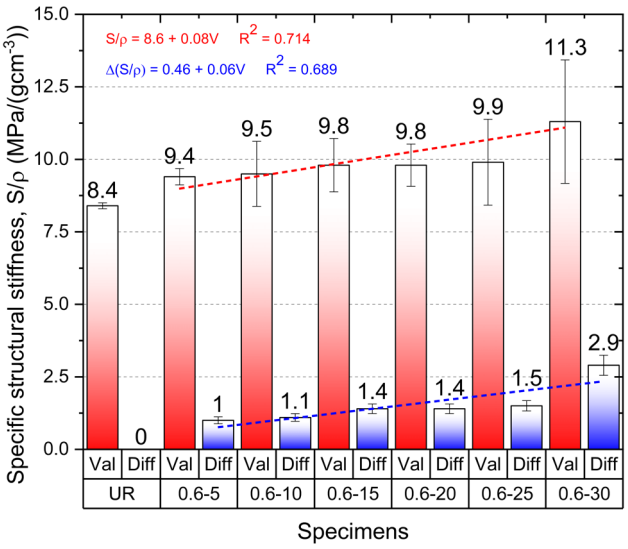


**Fig. 10** The specific structural stiffness and its deviation from the unreinforced (UR) sample as a function of reinforcement particles' volume fraction

The typical failure modes of CHS filled, SiC particles reinforced MMSFs are shown in Fig. 11, for the 0.6–15 sample, but all examined cases were summarized in Appendix E.

As shown in Fig. 11, the filler materials compressed and moved together with the matrix material, as indicated by the presence of ellipsoidal CHSs. The failure of the CHSs typically initiates at 5–10% engineering strain. At this stage of deformation, the main cleavage bands (red dashed lines), which split the samples into two halves, do not usually form at an exact angle of 45° with respect to the loading direction. Secondary cleavage bands (yellow dashed lines) also appeared in all cases.

Due to the increasing deformation rate, the cleavage zone widens. During the process, more and more CHSs were destroyed, and friction between the two halves, along with their large plastic deformation, contributed to the high energy absorption capacity. This process occurred at relatively high plateau stress levels, leading to enhanced energy absorption. As shown in Fig. 11, part of the specimen remained intact, with unbroken CHSs observed at nearly 50% deformation. This indicates that sliding occurred between the two halves of the specimen, meaning that the input mechanical energy was not fully utilized for material deformation. Consequently, the energy absorption efficiency was reduced.

## 4 Conclusions

In summary, Al99.5 matrix rMMSFs were successfully produced by liquid-state, low-pressure vacuum infiltration. Ceramic hollow spheres were applied as filler material with an Ø2.24±0.13 mm diameter, 0.87±0.08 gcm$^{-3}$ bulk density, and a 64% volume fraction. SiC particles with 0.597±0.11 mm size range (0.6 mm nominal size) were used as reinforcement. The main factor that was varied in our research was the volume fraction of the reinforcing material relative to the matrix material's volume: seven different volume fractions were investigated: 0 vol%, 5 vol%, 10 vol%, 15 vol%, 20 vol%, 25 vol% and 30 vol%, respectively. The samples were investigated structurally (microstructure) and tested mechanically (compressive test according to ISO13314:2011 [3]).

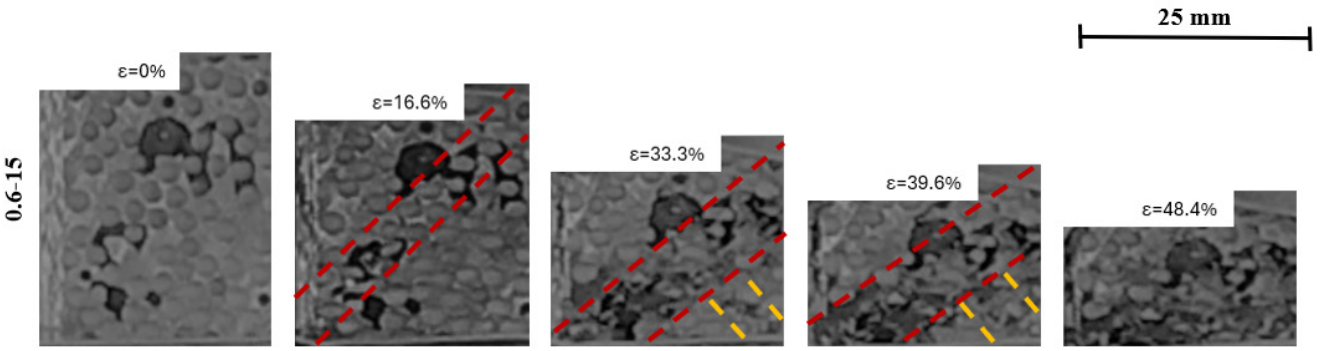


**Fig. 11** The failure modes of CHS filled, SiC particles reinforced MMSFs in the case of 0.6-15 sample

From the investigations carried out, the following conclusions can be drawn.

- Based on microstructural investigations, the matrix material uniformly filled the spaces between the filler and the SiC reinforcement particles. There were no signs of chemical interactions, matrix penetration into the filler, or any agglomeration of the filler or the reinforcing phase. It can be concluded that the liquid-state, low-pressure vacuum infiltration is a suitable production method for rMMSFs.
- The engineering stress-strain diagrams follow the classic behavior of CHS-filled MMSFs. The first peaks in the stress-strain diagrams were followed by sudden and significant drops. After this, the plateau strength region of the curves increased continuously.
- The specific compressive strength and the specific structural stiffness of the rMMSFs significantly increased in every case. Still, the increase in the specific plateau strength and the specific energy absorption of the samples was achieved in a higher reinforcement volume fraction.
- A linear relationship was found between every specific mechanical property and the volume fraction of the reinforcing particles, with $R^2$ between 0.55 and 0.9.
- The rMMSFs' matrix material was already a composite material, so the difference in strength between the matrix and the filler materials was smaller. As a result, the matrix material was able to withstand substantially higher stresses, thereby reducing the load transferred to the filler. Consequently, the failure of the CHSs occurred at significantly higher stress than in the case of the unreinforced matrices.
- The plateau region of the rMMSFs was influenced by the reinforcing particles. In a case of lower volume fraction values (5 vol% – 10 vol%), the structural integrity may be disrupted. Only higher reinforcement contents (≥ 15 vol%) begin to behave as reinforcing elements and increase the plateau strength.
- Based on the rMMSFs' mechanical properties, significant improvements can be achieved in every mechanical property usage of min. 15 vol% reinforcing particles.
- The failure mode of rMMSFs was dependent on the dual composite nature of the samples. The reinforced syntactic foams' failure was caused by plastic deformation with the appearance of a cleavage band and its widening.

**Acknowledgement**

This work was supported by the National Research, Development and Innovation Office (NKFIH), under grant agreement OTKA-FK_21 138505. Project no. TKP-6-6/PALY-2021 has been implemented with the support provided by the Ministry of Culture and Innovation of Hungary from the National Research, Development and Innovation Fund, financed under the TKP2021-NVA funding scheme.

## References

[1] Movahedi, N., Fiedler, T., Taşdemirci, A., Murch, G. E., Belova, I. V., Güden, M. "Impact loading of functionally graded metal syntactic foams", Materials Science and Engineering: A, 839, 142831, 2022. https://doi.org/10.1016/j.msea.2022.142831

[2] Thalmaier, G., Sechel, N.A., Csapai, A., Popa, C. O., Batin, G., Gábora, A., Mankovits, T., Vida-Simiti, I. "Aluminum Perlite Syntactic Foams", Materials, 15(15), 5446, 2022. https://doi.org/10.3390/ma15155446

[3] Jung, J., Kim, S., Kang, J., Park, J., Kim, W., Lim, C., Park, Y. "Compressive strength modeling and validation of cenosphere-reinforced aluminum–magnesium-matrix-based syntactic foams", Materials Science and Engineering: A, 849, 143452, 2022. https://doi.org/10.1016/j.msea.2022.143452

[4] Su, M., Li, J., Li, M.,Hao, H. "Microstructure and mechanical properties of bimodal syntactic foams with different size combination and volume fraction of alumina hollow spheres", Materials Science and Engineering: A, 824, 141798, 2021. https://doi.org/10.1016/j.msea.2021.141798

[5] Varga. D., Szlancsik, A. "Investigation of the Effect of Heat Treatment Time in Case of Recrystallization of Al99.5", Periodica Polytechnica Mechanical Engineering, 67(3), pp. 252–258, 2023 https://doi.org/10.3311/PPme.22823

[6] Anbuchezhiyan, G., Muthuramalingam, T., Mohan, B. "Effect of process parameters on mechanical properties of hollow glass microsphere reinforced magnesium alloy syntactic foams under vacuum die casting", Archives of Civil and Mechanical Engineering, 18(4), pp. 1645–1650, 2018. https://doi.org/10.1016/j.acme.2018.07.008

[7] Kubelka, P., Kádár, C., Jost, N. "Effect of the interface on the compressive properties of magnesium syntactic foams", Materials Letters, 287, 129293, 2021. https://doi.org/10.1016/j.matlet.2020.129293

[8] Anbuchezhiyan, G., Mohan, B., Sathianarayanan, D., Muthuramalingam, T, "Synthesis and characterization of hollow glass microspheres reinforced magnesium alloy matrix syntactic foam", Journal of Alloys and Compounds, 719, pp. 125–132, 2017. https://doi.org/10.1016/j.jallcom.2017.05.153

[9] Braszczyńska-Malik, K. N., Kamieniak, J. "AZ91 magnesium matrix foam composites with fly ash cenospheres fabricated by negative pressure infiltration technique", Materials Characterization, 128, pp. 209–216, 2017. https://doi.org/10.1016/j.matchar.2017.04.005

[10] Gupta, N., Luong, D. D., Cho, K. "Magnesium Matrix Composite Foams—Density, Mechanical Properties, and Applications", Metals, 2(3), pp. 238–252, 2012. https://doi.org/10.3390/met2030238

[11] Samvatsar, K., Dave, H. "A comprehensive study on using fly ash as reinforcement material in aluminium and magnesium based syntactic foams", Materials Today: Proceedings, 47, pp. 2384–2390, 2021. https://doi.org/10.1016/j.matpr.2021.04.353

[12] Castro, G., Nutt, S. R. "Synthesis of syntactic steel foam using mechanical pressure infiltration", Materials Science and Engineering: A, 535, pp. 274–280, 2012. https://doi.org/10.1016/j.msea.2011.12.084

[13] Jain, H., Mondal, D.P., Gupta, G., Kumar, R., Singh, S. "Synthesis and characterization of 316L stainless steel foam made through two different removal process of space holder method", Manufacturing Letters, 26, pp. 33–36, 2020. https://doi.org/10.1016/j.mfglet.2020.09.005

[14] Rabiei, A., Garcia-Avila, M. "Effect of various parameters on properties of composite steel foams under variety of loading rates", Materials Science and Engineering: A, 564, pp. 539–547, 2013. https://doi.org/10.1016/j.msea.2012.11.108

[15] Castro, G., Nutt, S. R. "Synthesis of syntactic steel foam using gravity-fed infiltration", Materials Science and Engineering: A, 553, pp. 89–95, 2012. https://doi.org/10.1016/j.msea.2012.05.097

[16] Yang, Q., Yu, B., Hu, H., Hu, G., Miao, Z., Wei, Y., Sun, W. "Melt flow and solidification during infiltration in making steel matrix syntactic foams", Materials Science Technology, 35(15), pp. 1831–1839, 2019. https://doi.org/10.1080/02670836.2019.1650444

[17] Rabiei, A., Karimpour, K., Basu, D., Janssens, M. "Steel-steel composite metal foam in simulated pool fire testing", International Journal of Thermal Sciences, 153, 106336, 2020. https://doi.org/10.1016/j.ijthermalsci.2020.106336

[18] Mei, Y., Fu, C., Fu, Y., Ding, Y.,Wang, E., Yang, Q. "Tensile Behavior and Performance of Syntactic Steel Foams Prepared by Infiltration Casting", Metals, 12(4), 668, 2022. https://doi.org/10.3390/met12040668

[19] N. Jha, D. P. Mondal, M. D. Goel, J. D. Majumdar, S. Das, O. P. Modi, "Titanium cenosphere syntactic foam with coarser cenosphere fabricated by powder metallurgy at lower compaction load", Transactions of Nonferrous Metals Society of China, 24(1), pp. 89–99, 2014. https://doi.org/10.1016/S1003-6326(14)63032-6

[20] Mondal, D. P., Majumder, J. D., Jha, N., Badkul, A., Das, S., Patel, A., Gupta, G. "Titanium-cenosphere syntactic foam made through powder metallurgy route", Materials & Design, 34, pp. 82–89, 2012. https://doi.org/10.1016/j.matdes.2011.07.055

[21] Xue, X., Zhao, Y. "Ti matrix syntactic foam fabricated by powder metallurgy: Particle breakage and elastic modulus", JOM, 63(2), pp. 43–47, 2011. https://doi.org/10.1007/s11837-011-0027-0

[22] Linul, E., Lell, D., Movahedi, N., Codrean, C.,Fiedler, T. "Compressive properties of zinc syntactic foams at elevated temperatures", Composites Part B: Engineering, 167, pp. 122–134, 2019. https://doi.org/10.1016/j.compositesb.2018.12.019

[23] Kemény, A., Katona, B., Movahedi, N.,Fiedler, T. "Fatigue tests of zinc aluminium matrix syntactic foams filled with expanded perlite", IOP Conference Series Materials Science Engineering, 903(1), 012050, 2020. https://doi.org/10.1088/1757-899X/903/1/012050

[24] Broxtermann, S., Vesenjak, M., Krstulović-Opara, L., Fiedler, T. "Quasi static and dynamic compression of zinc syntactic foams", Journal of Alloys and Compounds, 768, pp. 962–969, 2018. https://doi.org/10.1016/j.jallcom.2018.07.215

[25] Movahedi, N., Murch, G. E., Belova, I. V., Fiedler, T. "Effect of Heat Treatment on the Compressive Behavior of Zinc Alloy ZA27 Syntactic Foam", Materials, 12(5), 792, 2019. https://doi.org/10.3390/ma12050792

[26] Cochran, J. K. "Ceramic hollow spheres and their applications", Current Opinion in Solid State and Materials Science, 3(5), pp. 474–479, 1998. https://doi.org/10.1016/S1359-0286(98)80010-7

[27] Maria, J. A. S., Schultz, B. F., Ferguson, J. B., Rohatgi, P. K. "Al–Al2O3 syntactic foams – Part I: Effect of matrix strength and hollow sphere size on the quasi-static properties of Al-A206/Al2O3 syntactic foams", Materials Science and Engineering: A, 582, pp. 415–422, 2013. https://doi.org/10.1016/j.msea.2013.05.081

[28] Ferguson, J. B., Maria, J. A. S., Schultz, B. F., Rohatgi, P. K. "Al–$Al_2O_3$ syntactic foams—Part II: Predicting mechanical properties of metal matrix syntactic foams reinforced with ceramic spheres", Materials Science and Engineering: A, 582, pp. 423–432, 2013
https://doi.org/10.1016/j.msea.2013.06.065

[29] Omar, M. Y., Xiang, C., Gupta, N., Strbik, O. M., Cho, K. "Data characterizing flexural properties of Al/$Al_2$ $O_3$ syntactic foam core metal matrix sandwich", Data in Brief, 5, pp. 564–571, 2015
https://doi.org/10.1016/j.dib.2015.09.054

[30] Maria, J. A. S., Schultz, B. F., Ferguson, J. B., Gupta, N., Rohatgi, P. K. "Effect of hollow sphere size and size distribution on the quasi-static and high strain rate compressive properties of Al-A380–$Al_2O_3$ syntactic foams", Journal of Materials Science, 49(3), pp. 1267–1278, 2014.
https://doi.org/10.1007/s10853-013-7810-y

[31] Su, M.M., Wang, H., Li, K.Y., Hao, H. "Microstructure and Compressive Properties of Al/Al2O3 Syntactic Foams", Materials Science Forum, 933, pp. 174–181, 2018.
https://doi.org/10.4028/www.scientific.net/MSF.933.174

[32] Sripathy, A. P., Handjaja, C., Manakari, V., Parande, G., Gupta, M. "Development of Lightweight Magnesium/Glass Micro Balloon Syntactic Foams Using Microwave Approach with Superior Thermal and Mechanical Properties", Metals, 11(5), 827, 2021
https://doi.org/10.3390/met11050827

[33] Lehmhus, D., Weise, J., Baumeister, J., Peroni, L., Scapin, M., Fichera, C., Avalle, M., Busse, M. "Quasi-static and Dynamic Mechanical Performance of Glass Microsphere- and Cenosphere-based 316L Syntactic Foams", Procedia Materials Science, 4, pp. 383–387, 2014.
https://doi.org/10.1016/j.mspro.2014.07.578

[34] Lin, Y., Zhang, Q., Wu, G. "Interfacial microstructure and compressive properties of Al–Mg syntactic foam reinforced with glass cenospheres", Journal of Alloys and Compounds, 655, pp. 301–308, 2016.
https://doi.org/10.1016/j.jallcom.2015.09.175

[35] L. Vendra, B. Neville, and A. Rabiei, "Fatigue in aluminum–steel and steel–steel composite foams", Materials Science and Engineering: A, 517(1–2), pp. 146–153, 2009.
https://doi.org/10.1016/j.msea.2009.03.075

[36] Qin, R., Guo, C., Jiang, F., Li, Y., Cao, M., Guo, D. "Effect of sintering temperature on microstructure characteristics and damping capacity of multilayer 316L stainless steel hollow spheres/A356 alloy composites reinforced by NiTi alloy sheets", Materials Science and Engineering: A, 860, 144321, 2022.
https://doi.org/10.1016/j.msea.2022.144321

[37] Vendra L. J., Rabiei, A. "A study on aluminum–steel composite metal foam processed by casting", Materials Science and Engineering: A, 465(1–2), pp. 59–67, 2007.
https://doi.org/10.1016/j.msea.2007.04.037

[38] Taherishargh, M., Sulong, M. A., Belova, I. V., Murch, G. E., Fiedler, T. "On the particle size effect in expanded perlite aluminium syntactic foam", Materials & Design, 1980-2015, 66, pp. 294–303, 2015.
https://doi.org/10.1016/j.matdes.2014.10.073

[39] Borovinšek, M., Taherishargh, M., Vesenjak, M., Ren, Z., Fiedler, T. "Geometrical characterization of perlite-metal syntactic foam", Materials Characterization, 119, pp. 209–215, 2016.
https://doi.org/10.1016/j.matchar.2016.07.024

[40] Kádár, C., Chmelík, F., Ugi, D., Máthis, K., Knapek, M. "Damage Characterization during Compression in a Perlite-Aluminum Syntactic Foam", Materials, 12(20), p. 3342, 2019.
https://doi.org/10.3390/ma12203342

[41] Broxtermann, S., Taherishargh, M., Belova, I. V., Murch, G. E., Fiedler, T. "On the compressive behaviour of high porosity expanded Perlite-Metal Syntactic Foam (P-MSF)", Journal of Alloys and Compounds, 691, pp. 690–697, 2017.
https://doi.org/10.1016/j.jallcom.2016.08.284

[42] Taherishargh, M., Katona, B., Fiedler, T., Orbulov, I. N. "Fatigue properties of expanded perlite/aluminum syntactic foams", Journal of Composite Materials, 51(6), pp. 773–781, 2017.
https://doi.org/10.1177/0021998316654305

[43] Sulong, M. A., Taherishargh, M., Belova, I. V., Murch, G. E., Fiedler, T. "On the mechanical anisotropy of the compressive properties of aluminium perlite syntactic foam", Computational Materials Science, 109, pp. 258–265, 2015.
https://doi.org/10.1016/j.commatsci.2015.07.038

[44] Wright, A., Kennedy, A. "The Processing and Properties of Syntactic Al Foams Containing Low Cost Expanded Glass Particles", Advanced Engineering Materials, 19(11), 1600467, 2017
https://doi.org/10.1002/adem.201600467

[45] Broxtermann, S., Su, M. M., Hao, H., Fiedler, T. "Comparative study of stir casting and infiltration casting of expanded glass-aluminium syntactic foams", Journal of Alloys and Compounds, 845, 155415, 2020.
https://doi.org/10.1016/j.jallcom.2020.155415

[46] Su, M., Wang, H., Hao, H., Fiedler, T. "Compressive properties of expanded glass and alumina hollow spheres hybrid reinforced aluminum matrix syntactic foams", Journal of Alloys and Compounds, 821, 153233, 2020.
https://doi.org/10.1016/j.jallcom.2019.153233

[47] Al-Sahlani, K., Taherishargh, M., Kisi, E., Fiedler, T. "Controlled Shrinkage of Expanded Glass Particles in Metal Syntactic Foams", Materials, 10(9), 1073, 2017.
https://doi.org/10.3390/ma10091073

[48] Bonabi, S. B., Khabushan, J. K., Kahani, R., Raouf, A. H. "Fabrication of metallic composite foam using ceramic porous spheres "Light Expanded Clay Aggregate' via casting process", Materials & Design, 64, pp. 310–315, 2014.
https://doi.org/10.1016/j.matdes.2014.07.061

[49] Movahedi, N., Linul, E. "Mechanical properties of Light Expanded Clay Aggregated (LECA) filled tubes", Materials Letters, 217, pp. 194–197, 2018.
https://doi.org/10.1016/j.matlet.2018.01.078

[50] Puga, H., Carneiro, V. H., Jesus, C., Pereira, J., Lopes, V. "Influence of particle diameter in mechanical performance of Al expanded clay syntactic foams", Composite Structures, 184, pp. 698–703, 2018.
https://doi.org/10.1016/j.compstruct.2017.10.040

[51] Szlancsik, A., Kincses, D., Orbulov, I. N. "Mechanical properties of AlSi10MnMg matrix syntactic foams filled with lightweight expanded clay particles", IOP Conference Series: Materials Science and Engineering, 903, 012045, 2020.
https://doi.org/10.1088/1757-899X/903/1/012045

[52] Kemény, A., Leveles, B., Károly, D. "Functional aluminium matrix syntactic foams filled with lightweight expanded clay aggregate particles", Materials Today: Proceedings, 45(Part 5), pp. 4229 4232, 2021. https://doi.org/10.1016/j.matpr.2020.12.164

[53] Su, M., Wang, H., Hao, H. "Compressive Properties of Aluminum Matrix Syntactic Foams Prepared by Stir Casting Method", Advanced Engineering Materials, 21(8), 1900183, 2019. https://doi.org/10.1002/adem.201900183

[54] Rajan, T. P. D., Pillai, R. M., Pai, B. C. , Satyanarayana, K. G., Rohatgi, P. K. "Fabrication and characterisation of Al–7Si–0.35Mg/fly ash metal matrix composites processed by different stir casting routes", Composites Science and Technology, 67(15–16), pp. 3369–3377, 2007. https://doi.org/10.1016/j.compscitech.2007.03.028

[55] Mondal, D. P. , Das, S., Ramakrishnan, N., Bhasker, K. U. "Cenosphere filled aluminum syntactic foam made through stir-casting technique", Composites Part A: Applied Science and Manufacturisng, 40(3), pp. 279–288, 2009. https://doi.org/10.1016/j.compositesa.2008.12.006

[56] Du, W., Orbulov, I. N., Tamás-Bényei, P., Kádár, C. "Mechanical Behavior of Layered Composite Structures of Aluminum Foam Partially Filled with Polyamide", Periodica Polytechnica Mechanical Engineering, 69(2), pp. 164–170, 2025. https://doi.org/10.3311/PPme.40446

[57] Vogiatzis, C. A., Tsouknidas, A., Kountouras, D. T.,Skolianos, S. "Aluminum–ceramic cenospheres syntactic foams produced by powder metallurgy route", Materials & Design, 85, pp. 444–454, 2015. https://doi.org/10.1016/j.matdes.2015.06.154

[58] Huang, W., Liu, G., Li, H., Wang, F., Wang, Y. "Compressive Properties and Failure Mechanisms of Gradient Aluminum Foams Prepared by a Powder Metallurgy Method", Metals, 11(9), 1337, 2021. https://doi.org/10.3390/met11091337

[59] Pan, L., Rao, D., Yang, Y. Qiu, J., Sun, J., Gupta, N., Hu, Z."Gravity casting of aluminum-$Al_2O_3$ hollow sphere syntactic foams for improved compressive properties", Journal of Porous Materials, 27(4), pp. 1127–1137, 2020. https://doi.org/10.1007/s10934-020-00889-x

[60] Rajak, D. K., Mahajan, N. N., Linul, E. "Crashworthiness performance and microstructural characteristics of foam-filled thin-walled tubes under diverse strain rate", Journal of Alloys and Compounds, 775, pp. 675–689, 2019. https://doi.org/10.1016/j.jallcom.2018.10.160

[61] Linul, E., Khezrzadeh, O. "Axial crashworthiness performance of foam-based composite structures under extreme temperature conditions", Composite Structures, 271, 114156, 2021. https://doi.org/10.1016/j.compstruct.2021.114156

[62] Linul, E., Pietras, D., Sadowski, T., Marşavina, L., Rajak, D. K., Kovacik, J. "Crashworthiness performance of lightweight Composite Metallic Foams at high temperatures", Composites Part A: Applied Science and Manufacturing, 149, 106516, 2021. https://doi.org/10.1016/j.compositesa.2021.106516

[63] Song, J., Xu, S., Xu, L., Zhou, J., Zou, M. "Experimental study on the crashworthiness of bio-inspired aluminum foam-filled tubes under axial compression loading", Thin-Walled Structures, 155, 106937, 2020. https://doi.org/10.1016/j.tws.2020.106937

[64] Marx, J., Portanova, M., Rabiei, A. "Performance of Composite Metal Foam Armors against Various Threat Sizes", Journal of Composites Science, 4(4),176, 2020. https://doi.org/10.3390/jcs4040176

[65] Marx, J., Portanova, M.,Rabiei, A. "Ballistic performance of composite metal foam against large caliber threats", Composite Structures, 225, 111032, 2019. https://doi.org/10.1016/j.compstruct.2019.111032

[66] Garcia-Avila, M., Portanova, M., Rabiei, A. "Ballistic performance of composite metal foams", Composite Structures, 125, pp. 202–211, 2015. https://doi.org/10.1016/j.compstruct.2015.01.031

[67] Mondal, D. P., Jha, N., Badkul, A., Das, S., Khedle, R. "High temperature compressive deformation behaviour of aluminum syntactic foam", Materials Science and Engineering: A, 534, pp. 521–529, 2012. https://doi.org/10.1016/j.msea.2011.12.002

[68] Manoj, Khan, D. M. A., Mondal, D. P. "High temperature deformation behavior of closed cell ZnAl27 hybrid foam made through stir casting technique", Materials Science and Engineering :A, 731, pp. 324–330, 2018. https://doi.org/10.1016/j.msea.2018.06.044

[69] Fehér, A., Maróti, J. E., Takács, D. M., Orbulov, I. N., Kovács, R. "Thermal and mechanical properties of AlSi7Mg matrix syntactic foams reinforced by $Al_2O_3$ or SiC particles in matrix", International Journal of Heat and Mass Transfer,226, 125446, 2024. https://doi.org/10.1016/j.ijheatmasstransfer.2024.125446

[70] Maróti, J. E., Orbulov, I. N. "Characteristic compressive properties of AlSi7Mg matrix syntactic foams reinforced by Al2O3 or SiC particles in the matrix", Materials Science and Engineering: A, 869, 144817, 2023. https://doi.org/10.1016/j.msea.2023.144817

[71] International Organization for Standardization '2011 - ISO133142011 "Mechanical testing of metals - Ductility testing - Compression test for porous and cellular metals",ISO, Geneva, Switzerland, 2021.

## Appendix A

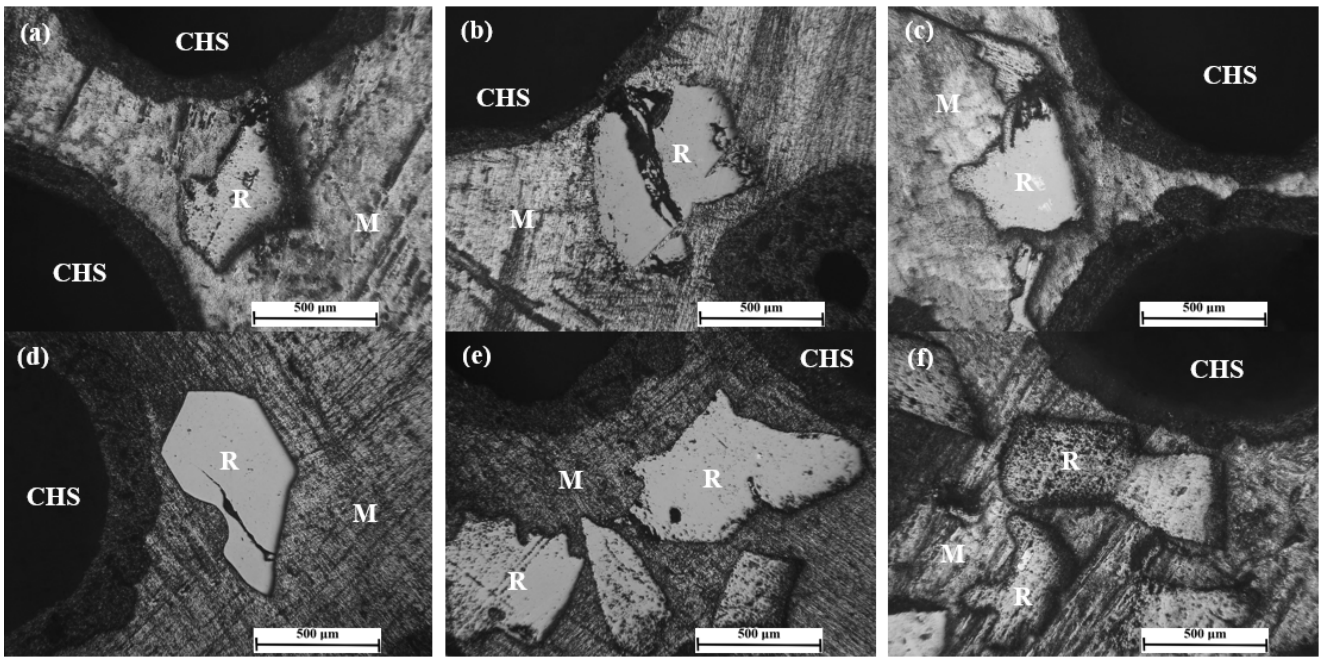


**Fig. A1** Microstructure of produced rMMSFs (a) 0.6-5, (b) 0.6-10, (c) 0.6-15, (d) 0.6-20, (e) 0.6-25, (f) 0.6-30 (M – matrix, R – reinforcing particles, CHS – ceramic hollow spheres – please note that not all the particles have been labeled)

## Appendix B

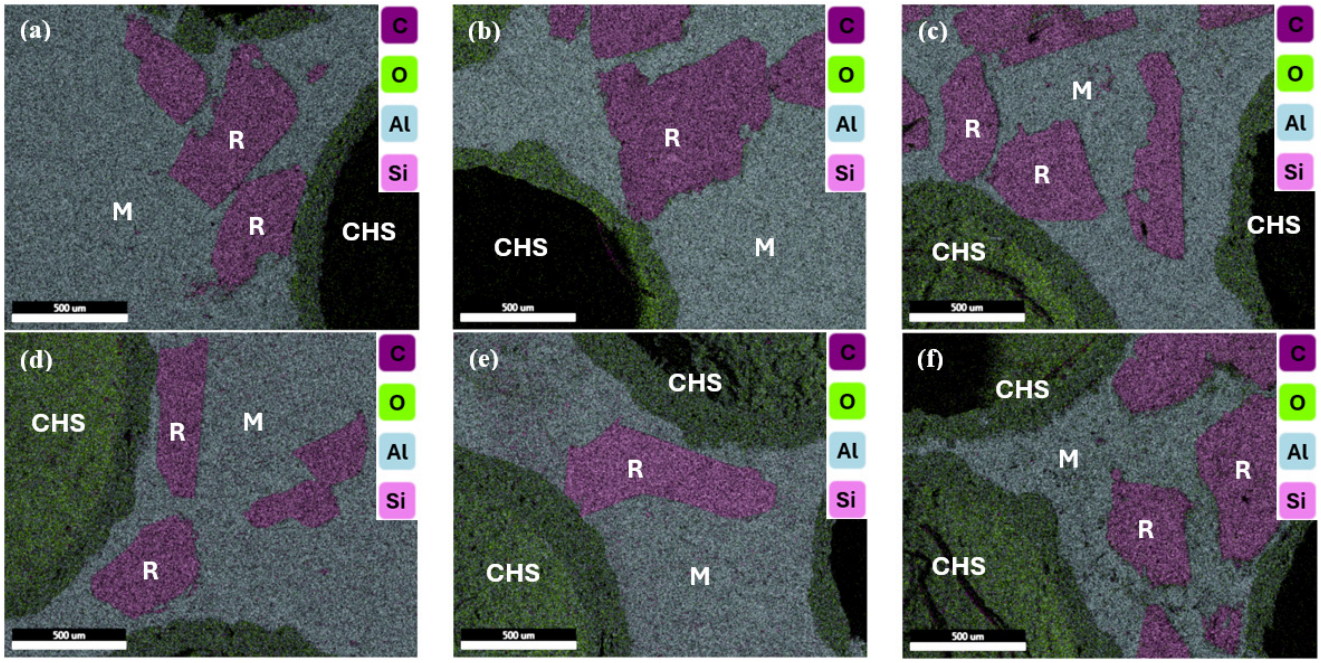


**Fig. B1** EDS map of the investigated rMMSF (a) 0.6-5, (b) 0.6-10, (c) 0.6-15, (d) 0.6-20, (e) 0.6-25, (f) 0.6-30 (M – matrix, R – reinforcing particles, CHS – ceramic hollow spheres – please note that not all the particles have been labeled)

## Appendix C

**Table C1** Mechanical properties (compressive strength ($\sigma_C$), plateau strength ($\sigma_{PLT}$), energy absorption ($W_{50}$), structural stiffness ($S$)) of investigated rMMSFs

| Designation | $\sigma_C$ (MPa) | $\sigma_{PLT}$ (MPa) | $W_{50}$ (Jcm$^{-3}$) | $S$ (MPa) |
|---|---|---|---|---|
| 0-0 | 50.8 ± 6.30 | 58.2 ± 6.40 | 27.9 ± 2.8 | 14.1 ± 0.17 |
| 0.6-5 | 68.2 ± 5.60 | 52.9 ± 3.45 | 25.3 ± 3.4 | 16.2 ± 0.42 |
| 0.6-10 | 74.1 ± 5.68 | 54.3 ± 4.21 | 27.4 ± 1.8 | 17.2 ± 2.44 |
| 0.6-15 | 79.8 ± 3.55 | 66.5 ± 4.89 | 32.0 ± 1.6 | 17.8 ± 1.95 |
| 0.6-20 | 81.6 ± 6.10 | 70.2 ± 10.39 | 33.2 ± 3.9 | 18.9 ± 1.89 |
| 0.6-25 | 84.7 ± 9.99 | 67.5 ± 11.83 | 32.9 ± 4.8 | 19.1 ± 4.01 |
| 0.6-30 | 94.2 ± 12.29 | 70.1 ± 8.33 | 34.2 ± 4.2 | 21.7 ± 5.38 |

## Appendix D

**Table D1** Specific mechanical properties (compressive strength ($\sigma_C$), plateau strength ($\sigma_{PLT}$), energy absorption ($W_{50}$), structural stiffness ($S$)) of investigated rMMSFs

| Designation | $\sigma_C/\rho$ (MPa/(gcm$^{-3}$)) | $\sigma_{PLT}/\rho$ (MPa /(gcm$^{-3}$)) | $W_{50}/\rho$ (J/g) | $S/\rho$ (MPa/(gcm$^{-3}$)) |
|---|---|---|---|---|
| 0-0 | 30.2 ± 2.90 | 34.6 ± 3.00 | 16.6 ± 1.5 | 8.4 ± 0.10 |
| 0.6-5 | 39.3 ± 2.99 | 30.5 ± 1.75 | 14.5 ± 1.9 | 9.4 ± 0.28 |
| 0.6-10 | 41.1 ± 2.17 | 30.2 ± 1.67 | 15.2 ± 0.7 | 9.5 ± 1.12 |
| 0.6-15 | 44.1 ± 1.15 | 36.7 ± 2.32 | 17.7 ± 0.7 | 9.8 ± 0.92 |
| 0.6-20 | 42.3 ± 2.37 | 36.2 ± 3.67 | 17.2 ± 1.2 | 9.8 ± 0.73 |
| 0.6-25 | 44.4 ± 2.94 | 35.2 ± 4.47 | 17.2 ± 1.6 | 9.9 ± 1.48 |
| 0.6-30 | 49.3 ± 4.07 | 36.7 ± 2.62 | 17.9 ± 1.4 | 11.3 ± 2.13 |

## Appendix E

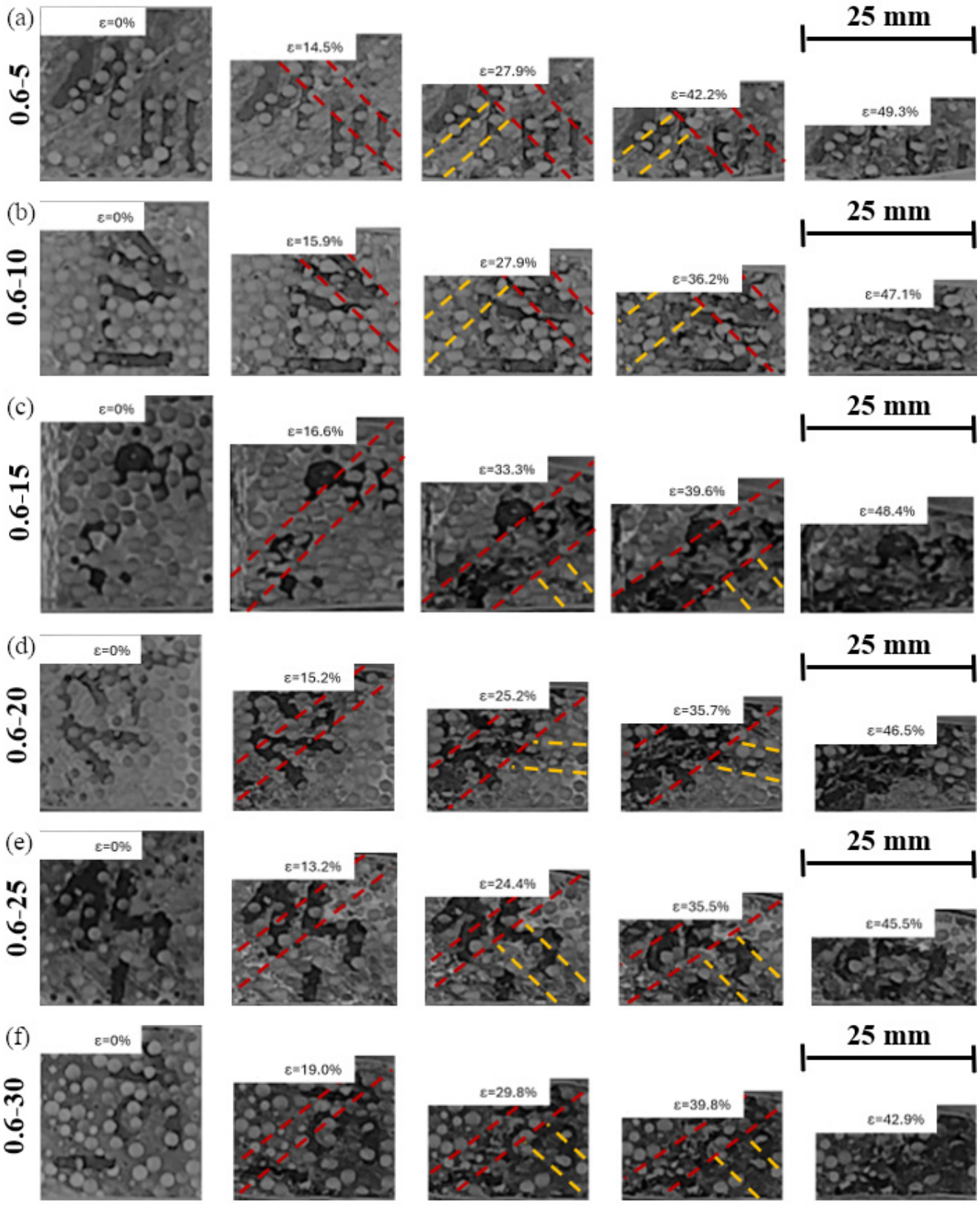


**Fig. E1** Failure modes of CHS filled and SiC particles reinforced metal matrix syntactic foams (a) 0.6-5, (b) 0.6-10, (c) 0.6-15, (d) 0.6-20, (e) 0.6-25, (f) 0.6-30